Ocean Sci. Discuss., https://doi.org/10.5194/os-2018-13
Manuscript under review for journal Ocean Sci.
Discussion started: 16 February 2018

Ocean Science Discussions

Some aspects of the deep abyssal overflow between the middle and southern basins of the Caspian Sea

Javad Babagoli Matikolaei [1], Abbasali Aliakbari Bidokhti [2], and Maryam Shiea [3]

[1]Graduate in Physical Oceanography, Institute of Geophysics, University of Tehran, Tehran, Iran.
[2] Institute of Geophysics, University of Tehran, Tehran, Iran.
[3] Faculty of Marine Science and Technology, Science and Research Branch, Islamic Azad University, Tehran, Iran.

Correspondence to: Abbasali Aliakbari Bidokhti (bidokhti@ut.ac.ir)

Abstract. This study investigates the deep gravity current between the middle and southern Caspian Sea basins, caused by density difference of deep waters. Oceanographic data, numerical model and dynamic models are used to consider the structure of this Caspian Sea abyssal overflow. The CTD data are obtained from UNESCO, and the three-dimensional ocean model COHERENS results are used to study the abyssal currents in the southern basin of the Caspian Sea.

The deep overflow is driven by the density difference mainly due to the temperature difference between the middle and southern basins especially in winter. For this reason, water sinks in high latitudes and after filling the middle basin it overflows into the southern basin. As the current passes through the Absheron Strait (or sill), we use an analytic model for the overflow gravity current with inertial effects, bottom friction and entrainment, to consider its structure. The dynamical characteristics of this deep baroclinic flow are investigated with different initial and boundary conditions. The results show that after time passes, the flow adjusts itself, moving as a deepening gravity driven topographically trapped current. This flow is considered for different seasons and its velocity and width are obtained. Because of the topography of the Southern Caspian basin, the flow is trapped after the sill; thus, another simple dynamical model of the overflow, based on potential vorticity similar to that of Bidokhti and Ezam (2009) but with the bottom friction and entrainment included, is used to find the horizontal extent of the outflow from the western coast. To estimate the changes of vorticity and potential vorticity of the flow over the Absheron sill, we use the method of Falcini and Salusti (2015), in this work, the effects of entrainment and friction are considered. Because of the importance of the overflow in deep water ventilation, a simple dynamical model of the boundary currents based on the shape of strait is used to estimate typical mass transport and flushing time which is found to be about 15 to 20 years for the southern basin of the Caspian Sea. This time scale is important for the possible effects on the ecosystem here of pollution due to oil exploration.

Keywords: Overflow, dynamical model, trapped baroclinic bottom current, Caspian Sea abyssal flow.

Ocean Sci. Discuss., https://doi.org/10.5194/os-2018-13
Manuscript under review for journal Ocean Sci.
Discussion started: 16 February 2018

1. Introduction

Baroclinic flows play important roles in ocean and sea circulations, especially in deep waters of the ocean. Because these currents are important in deep water ventilations of the oceans, they have an integral role in thermocline circulation. Vertical ocean circulation that is created by density differences and controlled by changes in surface temperature and salinity is known as thermohaline circulation. A driving mechanism for the circulation is the cooling of surface waters at high latitudes and consequent formations of deep waters by sinking the cooled salty water masses (Fogelqvist et al., 2003).

Cooling in polar seas (Dickson et al., 1990) and evaporation in marginal seas (Baringer and Price, 1997) cause dense waters that sink to form deep water masses. For example, dense water from the deep convective regions of the North Atlantic produces a signature of the thermohaline overturning circulation that can be seen as far away as the Pacific and Indian oceans (Girton et al., 2003). In the global sense, bottom-trapped currents play an integral role in thermohaline circulation and are a vehicle for the transport of heat, salt, oxygen and nutrients over great distances and depths. The ability of abyssal flows to transport and deposit sediments is also of geological interest (Smith, 1975). As thermohaline circulation causes ventilation of deep ocean water, it is important not only in open seas and ocean but also in semi-closed and closed basins ventilations. Study of thermohaline dynamics and circulation has also been of interest to other scientists such as climate researchers. The dynamics of such dense currents on slopes have been modelled in the past both theoretically and experimentally starting with Ellison and Turner (1959) and Britter and Linden (1980), and a review on gravity currents can be found in Griffiths (1986).

Bidokhti and Ezam (2009) presented a simple dynamical model of the outflow from the Persian Gulf based on potential vorticity conservation to find the horizontal extent of the outflow from the coast.

The Caspian Sea, the world's largest inland enclosed water body, consists of three basins namely northern (shallow, mean depth of about 10 m and covering 80000 km^2), the middle (rather deep, with mean depth of about 200 m, maximum depth 788 m and covering 138000 km^2) and the southern (deep, with a mean depth of 350 m, maximum depth 1025 m and covering 164840 km^2) and is located between 36.5 N and 47.2N, and 46.5E and 54.1E (Aubrey et al., 1994; Aubrey, 1994). The depth varies greatly over this sea (Ismailova, 2004, Figure 2). The northern basin, after a sudden depth transition at the shelf edge, reaches the middle one. The middle and southern basins are divided by the Absheron sill or strait (with maximum depth of 180 m). The western slopes of the two deeper basins are fairly steep compared to the eastern slope (Gunduz and Özsoy, 2014). Peeters et al (2000) have also estimated the ages of waters of the Caspian Sea basins while considering the exchange between the middle and southern basins, based on chemical tracers and found typical ages of about 20 to 25 years depending on the exchange rates. This exchange rate seems to vary year by year that is dominated by atmospheric forcings.

The Caspian Sea is enclosed with tides being fairly weak and circulation in this sea is mainly due to wind and buoyancy, although some wave-driven flows also occur in coastal regions [Bondarenko, 1993; Ghaffari and Chegini, 2010; Ghaffari et al., 2013; Ibrayev et al., 2010; Terziev et al., 1992]. The seasonal circulation based on a coupled sea hydrodynamics, air–sea interaction and sea ice thermodynamics model of the Caspian Sea was investigated by Ibrayev et al (2010) and Gunduz and Özsoy, 2014). The effect of fresh water inflow to the Caspian Sea on seasonal variations of salinity and circulation (or flow)

Ocean Sci. Discuss., https://doi.org/10.5194/os-2018-13
Manuscript under review for journal Ocean Sci.
Discussion started: 16 February 2018

pattern of the Caspian Sea surface has also been studied using HYCOM model (Kara et al, 2010). These studies indicate that in north-eastern parts of the middle basin of this sea there are signs of sinking water in cold season. Such deep convection can lead to thermocline convection affected by side topography of these basins (middle and southern basins). These deep topographically influenced rotating flows constitute the abyssal circulation of the Caspian Sea.

The main aim of our work is to investigate some aspects of the abyssal flows in the southern Caspian Sea basin using CTD data and some simulations of a numerical model. Firstly, we explain why abyssal circulation can occur in the Caspian Sea, and then discuss the structure of the outflow (overflow) from the middle to the southern Caspian Sea over the Absheron sill. An analytical model for the overflow gravity current over the Absheron sill, with inertial and frictional effects, is then presented. After the flow passes over the Absheron sill, we present a new model for the structure of this flow using another analytical model based on potential vorticity, similar to that of Bidokhti and Ezam (2009) but the bottom friction and entrainment is included. We then calculate values of mass transport, flushing times, and discuss the pathway of gravity current in southern Caspian Sea basin.

2 Data used and results

2.1 Observational data

The sea surface temperature (SST) in the northern basin ranges from below zero under frozen ice in winter to 25–26 °C in summer, while more moderate variability occurs in the southern basin changing from 7–10 °C in winter to 25–29 °C in summer (Ibrayev et al., 2010). To illustrate the differences of surface temperatures of the middle, southern, and northern basins in various seasons, time series of surface temperatures are plotted using MODIS data from 2014 to 2015 in figure 1. In winter, the surface temperature difference between the northern and southern basin is approximately 16 °C. Apart from this, the Caspian Sea has low salinity. In deep water areas, salinity varies little with depth (12.80–13.08 psu), and the density stratification largely depends on temperature variation (Terziev et al., 1992). Hence, denser water of the middle basin, in comparison to that of the southern basin, is expected as will now be shown.

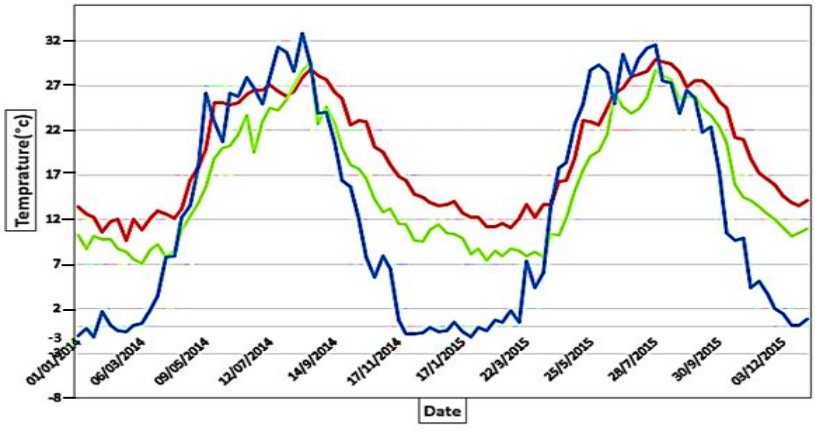

Figure 1: Comparison the surface temperature in Northern (Lat: 46.5°, Long: 50°) (blue), Middle (Lat: 39.5°, Long: 51°) (green), and Southern (Lat: 37°, Long: 52°) (red), basins of the Caspian Sea.

Ocean Sci. Discuss., https://doi.org/10.5194/os-2018-13
Manuscript under review for journal Ocean Sci.
Discussion started: 16 February 2018

The CTD data are obtained from UNESCO Atomic Energy International Agency, for summer 1996 (Figure 2). Vertical profiles of temperature, *T*, salinity, *S* and sigma-*T*, for the northern, middle, and southern Caspian Sea basins, show differences in temperature, salinity and sigma-*T* between these basins. Figure 3 shows typical vertical profiles of *T*, *S* and sigma-*T* in these basins (points a and b in Figure 2 right). Due to the density difference between the middle and southern basins, dense current crosses the Absheron sill. The cross-section of sigma-*T* shows that the abyssal gravity current moves from middle to southern basin (Figure 4). Not only in the Strait of Absheron are sigma-*T* contour gradients obvious but also there are contour gradients in southern basin, indicative of the northern overflow.

Due to the limited observational data, more extensive measurements and high resolution data are required to find the outflow structure and determine the analytical model parameters. For this reason, numerical model results have been used to do further analyses and also acquire the parameters of the overflow for the analytical model.

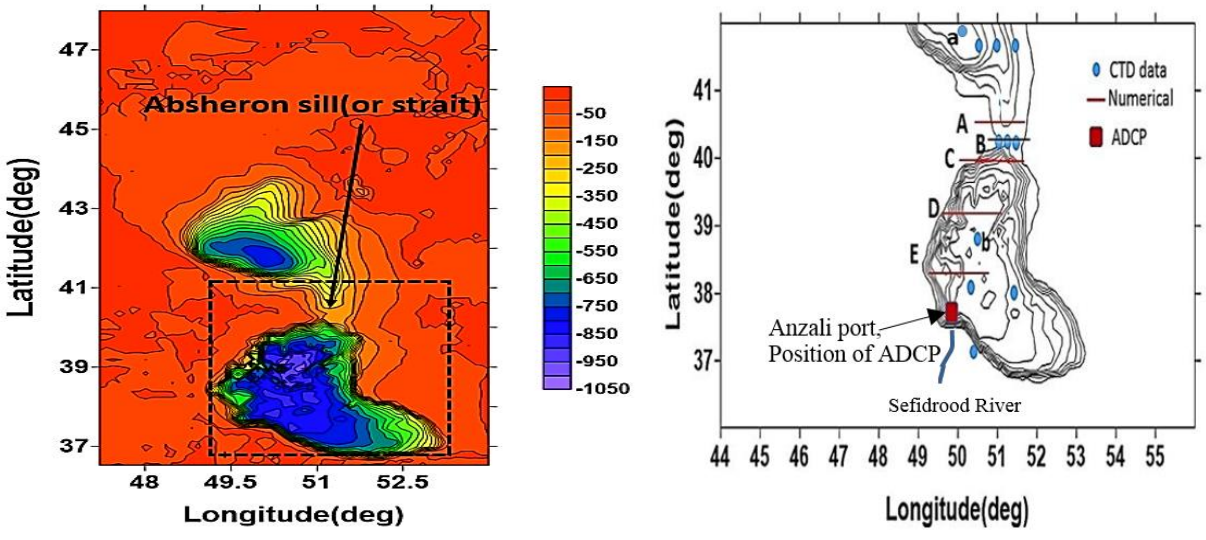

Figure 2: Schematic of the Caspian Sea and locations of CTD and ADCP measurements, the geographic position of transects (right), and topography of the basins, showing the Absheron sill (left).

Ocean Sci. Discuss., https://doi.org/10.5194/os-2018-13
Manuscript under review for journal Ocean Sci.
Discussion started: 16 February 2018

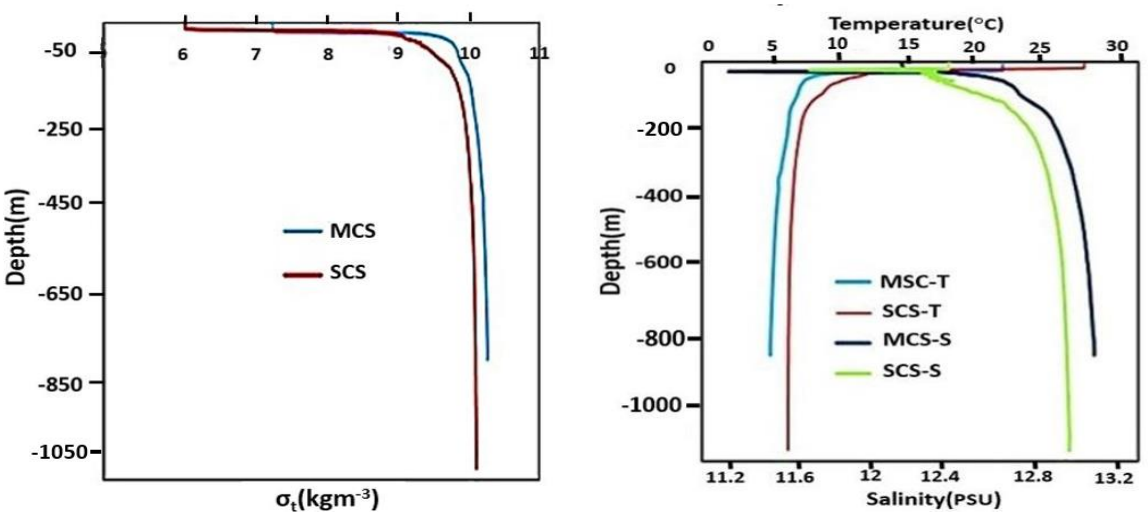

Figure 3: Comparison Salinity, *S* and temperature, *T* (right), and sigma-*T* (left) profiles between points a, in middle (MCS) and b, in southern (SCS) Caspian Sea basins (Figure 2 right).

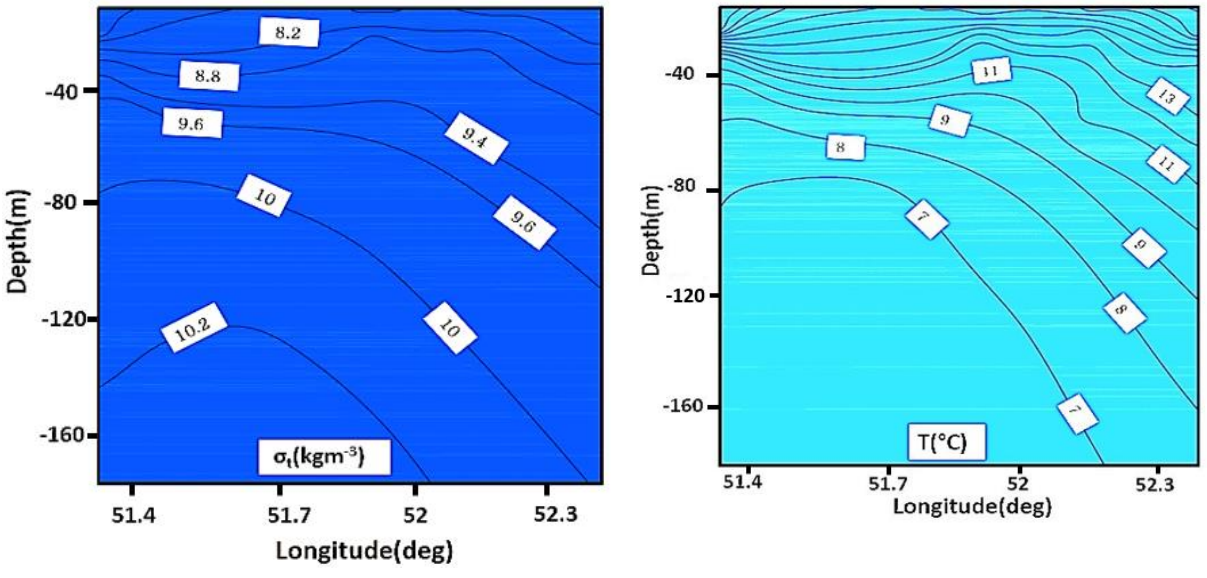

Figure 4: Observed sigma-*T* (left) and temperature (right) fields along transect B in summer, shown in Figure 2 right.

2.2 Some general features of the COHERENS numerical model, and its boundary and initial conditions

COHERENS (Coupled Hydrodynamical Ecological model for Regional Shelf seas; Luyten et al., 1999), has been used. COHERENS uses a vertical sigma coordinate and the hydrostatic incompressible version of the Navier-Stokes equations with

Ocean Sci. Discuss., https://doi.org/10.5194/os-2018-13
Manuscript under review for journal Ocean Sci.
Discussion started: 16 February 2018

Boussinesq approximation and equations of temperature and salinity. The model uses an Arakawa C-grid (Arakawa and Suarez, 1983), and equations are solved numerically using the mode-splitting technique. The grid size in horizontal is 0.046 × 0.046 degrees, typically 5 km, and 30 sigma levels, labelled k (the bottom layer is 1 and surface one is 30). The coastlines and bathymetry data with 0.5′ × 0.5′ resolution are acquired from GEBCO, although interpolated and smoothed slightly. The initialisation of the model was with January data; and it was forced by six hourly wind, acquired from ECMWF (Mazaheri et al., 2013), and air pressure and temperature with 0.5˚× 0.5˚ resolution acquired from ECMWF (ERA-Interim) reanalyses. Precipitation rate, cloud cover and relative humidity (2.5˚×2.5˚) were derived from NCEP/NCAR re-analysis data. The river inflows (from the Global Runoff Data Centre) were also included. The time steps of barotropic and baroclinic modes are 15 s and 150 s, respectively. The total simulation time is five years (from 2000 to 2004 inclusive) with six hour varying meteorological forcing and then the results of the last year are shown. The results of numerical model are validate by ADCP data between the estuary of the Sefidrood River and Anzali port (figure 2, 5). These data are collected by National Institute of Oceanography and Atmospheric Sciences, from November 2004 to the end of January 2005 (Shiea et al., 2016). This data was recorded by RCM9 current meters (at the ADCP station) at 3 depths on a mooring, near surface, 50 m, and 200 m. The simulation results of mean and long period variations of surface velocity components are rather consistent with observations. The difference in velocity between observation and model comes from some of the assumptions and the resolution used in the model as can be expected. The distance between two adjacent grid points in model is about 5 km and the ADCP data are a point in between two grid points, so interpolation are used to compare the model results with data of the point of observations.

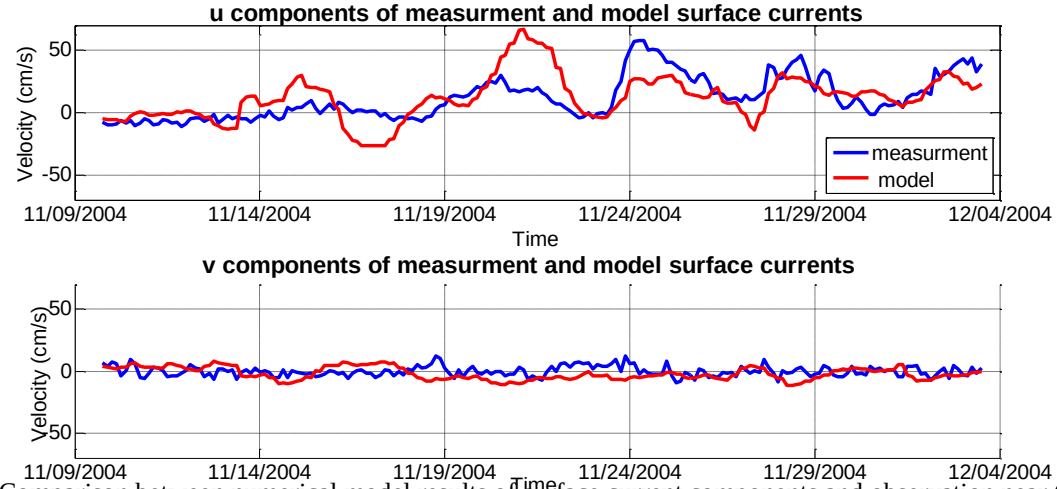

Figure 5: Comparison between numerical model results of surface current components and observation near the Sefidrood River and Anzali port (Shiea et al., 2016).

Typical numerical results of deep flows for the middle and southern basins of the Caspian Sea (the flow for the northern basin is not shown) for May and December of 2004, after four years of warm up of the model operation, are shown in Figure 6, 7 and 8. The deep narrow flow in the middle basin and the overflow over the Absheron sill and in the north western boundary of the southern basin are clearly observed. As the northern shallow waters of the Caspian Sea are subjected to high evaporation

Ocean Sci. Discuss., https://doi.org/10.5194/os-2018-13
Manuscript under review for journal Ocean Sci.
Discussion started: 16 February 2018

in summer, in the following cold seasons these waters become dense and start to sink, mainly in the north eastern side (Gunduz and Özsoy, 2014), into the middle basin(figure 6) . The flow due to its high density enters the deep part of the middle Caspian and starts to fill the middle Caspian Sea basin. After filling the middle Caspian basin, it appears to overflow into the southern basin, due to shape of Absheron strait that looks like a sill similar to Denmark Strait. This enters the southern Caspian Sea through Absheron. The topography has a strong effect on the deep basin flows. From such results the parameters of the deep flow are derived. There is a clear indication that the heavier water of the middle basin is overflowing near the bottom left towards the southern basin (figure 8).

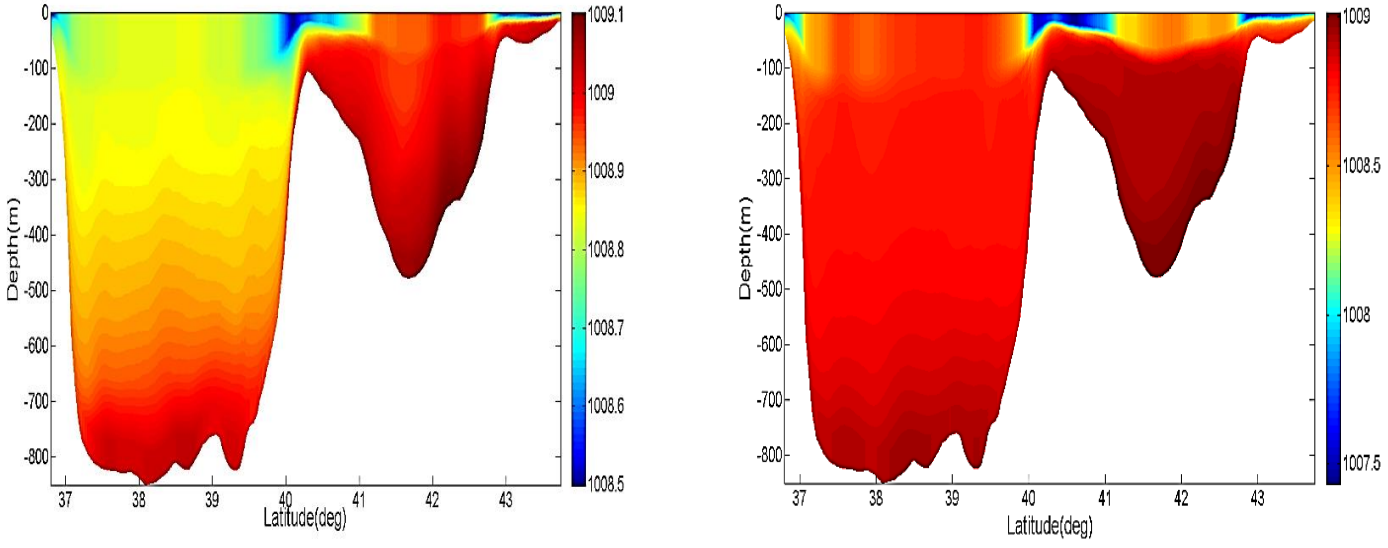

Figure 6: Cross-Section (N-S) of the mean density obtained from model simulation during September (left) and May (right).

Ocean Sci. Discuss., https://doi.org/10.5194/os-2018-13
Manuscript under review for journal Ocean Sci.
Discussion started: 16 February 2018

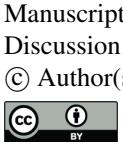

Ocean Science
Discussions
Open Access
EGU

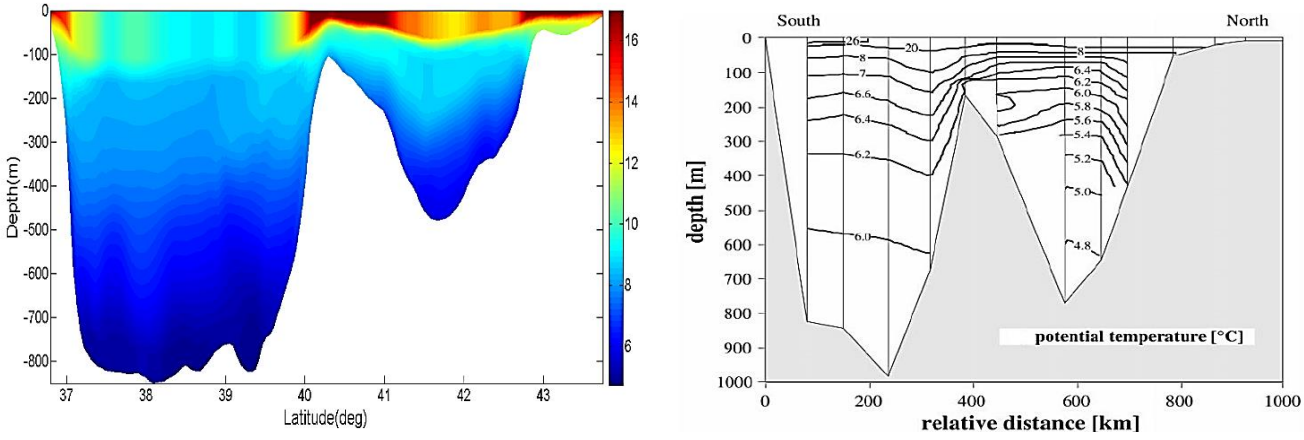

Figure 7: Comparison between Cross-sections (N-S) of the mean temperature obtained from model simulation (left) and Peeters et al (2000) studies (right) during September.

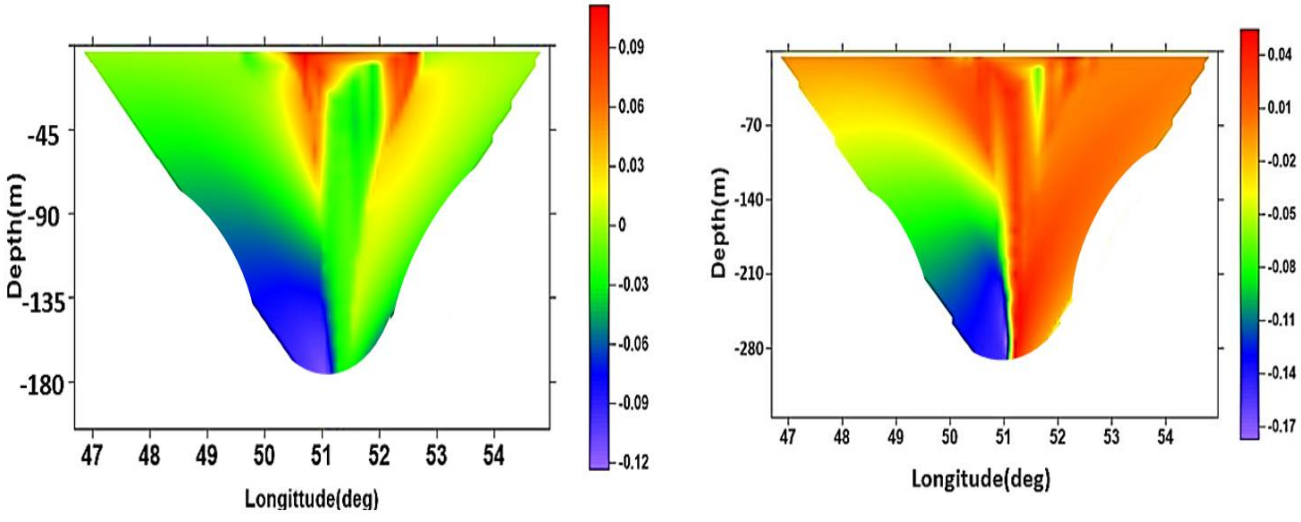

Figure 8: Cross-Section of the mean velocity (m/s) in transect A (left, for Jan.) and C (right, for May) obtained from model simulations.

The deep flow seems to follow the bottom topography, indicating that the deep side slopes of the middle and southern basins strongly influence the abyssal circulation. This in fact led us to propose an analytical model for the density current on a sloping bottom affected by bottom friction and entrainment, hence spiralling into the deep parts of the southern Caspian Sea basin. Typical Rossby number of this flow is about $Ro = \frac{U}{fW} = 0.2/(10^{-4} \times 20 \times 10^{3}) \sim 0.1$ (here U is typical speed of the overflow and W is its width), which justifies the geostrophic flow (assumption) entering the southern basin.

Ocean Sci. Discuss., https://doi.org/10.5194/os-2018-13
Manuscript under review for journal Ocean Sci.
Discussion started: 16 February 2018

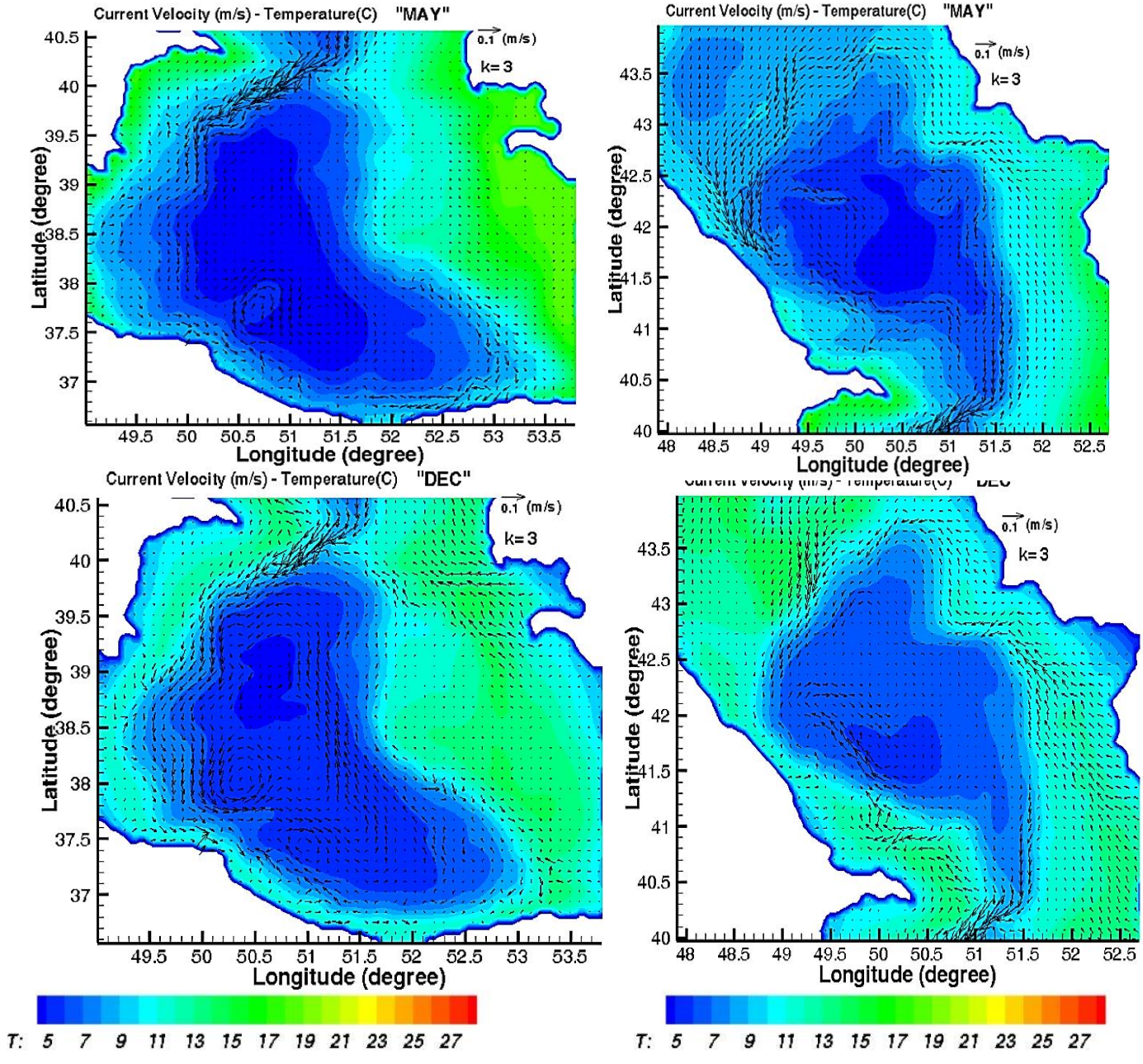

Figure 9: Monthly mean currents (m/s) in layer "k=3" (near the bottom) and temperature obtained from model simulations in southern (left) and middle (right) basins of the Caspian Sea for the months of May, December (2004).

Ocean Sci. Discuss., https://doi.org/10.5194/os-2018-13
Manuscript under review for journal Ocean Sci.
Discussion started: 16 February 2018

3 Dynamics of the overflow

3. 1 An analytical model for the overflow in the Strait

As the gravity current flows over the inclined sill, it adjusts itself under the gravitational, rotational and frictional forces. The zonal and meridional components of momentum of the buoyancy driven current are given by assuming no pressure gradient; a uniform dense flow under a less dense layer at rest; *x* coordinate is eastward and *y* is northward (see Figure 10); with entrainments at its boundaries, *E* (here solely as a frictional factor otherwise the flow becomes three dimensional and a similarity method would be suitable) and with bottom friction, τ_b; under these simplifying assumptions, the continuity equation is trivial and hence, the required momentum equations for the solution are:

$$\frac{du}{dt} = fv - \frac{\tau_{bx}}{\rho H} - \frac{E}{H}u$$
$$\frac{dv}{dt} = -fu - g'\tan\theta - \frac{\tau_{by}}{\rho H} - \frac{E}{H}v \qquad \textbf{(1)}$$

Where *u* and *v* are Lagrangian eastward and northward components of velocity respectively (Figure 10), *f* is the Coriolis parameter (= 2Ω sin υ, where Ω is the earth angular speed, and υ is the latitude angle), calculated as $f \sim 9.2\times10^{-5}$ s^{-1}. θ is the bottom slope angle and here tan θ=0.02, g' is the reduced gravity, values of reduced gravity were calculated for different seasons (see table 2) and *H* is the depth of overflow, about 50 to 70 m. The stress on the ocean bottom, τ_b, is parameterized by the usual quadratic form, $\tau_b=\rho C_d|U|u$ *or v* where C_d is drag coefficient and *U* is the magnitude of velocity. To simplify the analysis, we define $r_b = \frac{c_d|U|}{H}$ and $r_e = \frac{E}{H}$ .The solutions of these differential equations are as follows: (where *x* and *y* are Lagrangian location coordinates of the flow and c_1 and c_2 are constants to be found from initial conditions, see Table 2 below).

$$u(t) = c_1 e^{-(r_b+r_e)t}\cos(ft) + c_2 e^{-(r_b+r_e)t}\sin(ft) - \frac{g' f\tan\theta}{f^2+(r_b+r_e)^2}$$
$$v(t) = -c_1 e^{-(r_b+r_e)t}\sin(ft) + c_2 e^{-(r_b+r_e)t}\cos(ft) - \frac{g'(r_b+r_e)\tan\theta}{f^2+(r_b+r_e)^2} \qquad \textbf{(2)}$$
$$x(t) = \frac{fc_1-(r_b+r_e)c_2}{f^2+(r_b+r_e)^2}e^{-(r_b+r_e)t}\sin(ft) - \frac{fc_2+(r_b+r_e)c_1}{f^2+(r_b+r_e)^2}e^{-(r_b+r_e)t}\cos(ft) - \frac{g' f\tan\theta}{f^2+(r_b+r_e)^2}t + \frac{fc_2+(r_b+r_e)c_1}{f^2+(r_b+r_e)^2}$$
$$y(t) = \frac{fc_2+(r_b+r_e)c_1}{f^2+(r_b+r_e)^2}e^{-(r_b+r_e)t}\sin(ft) + \frac{fc_1-(r_b+r_e)c_2}{f^2+(r_b+r_e)^2}e^{-(r_b+r_e)t}\cos(ft) - \frac{g'(r_b+r_e)\tan\theta}{f^2+(r_b+r_e)^2}t + \frac{(r_b+r_e)c_2-fc_1}{f^2+(r_b+r_e)^2}$$

Where:

Ocean Sci. Discuss., https://doi.org/10.5194/os-2018-13
Manuscript under review for journal Ocean Sci.
Discussion started: 16 February 2018

$$c_2 = v_p + \frac{g'(r_b + r_e)\tan\theta}{f^2 + (r_b + r_e)^2}$$
$$c_1 = u_p + \frac{g' f \tan\theta}{f^2 + (r_b + r_e)^2} \quad \textbf{(3)}$$

u_p and v_p are components of velocity when the gravity current just begins to flow over the inclined sill.

As the time passes, the flow tends to reach a steady state and moves parallel to the sloped bed. Then in this situation $v_{t\to\infty}$ and $u_{t\to\infty}$ are obtained from the following equation in which μ is the flow angle from zonal east-west direction and λ is its initial value.

$$u_{t\to\infty} = -\frac{g' f \tan\theta}{f^2 + (r_b + r_e)^2}, v_{t\to\infty} = -\frac{g'(r_b + r_e)\tan\theta}{f^2 + (r_b + r_e)^2}$$
$$\tan\mu = \frac{v_{t\to\infty}}{u_{t\to\infty}}, \mu = \arctan\left(-\frac{r_b + r_e}{f}\right) \quad \textbf{(4)}$$
$$\tan\lambda = \frac{v_p}{u_p}, \lambda = \arctan\left(\frac{v_p}{u_p}\right)$$

As the flow develops with time it shows some oscillations with the local inertial period, and after a few inertial periods it acquires a steady state velocity namely $u_{t\to\infty}$ and $v_{t\to\infty}$. The analytical model input parameters (see Table 2 below) were determined from observations (cross-sections shown in Figure 4) and numerical simulations in the Strait of Absheron, from the cross-sections as shown in Figure 11.

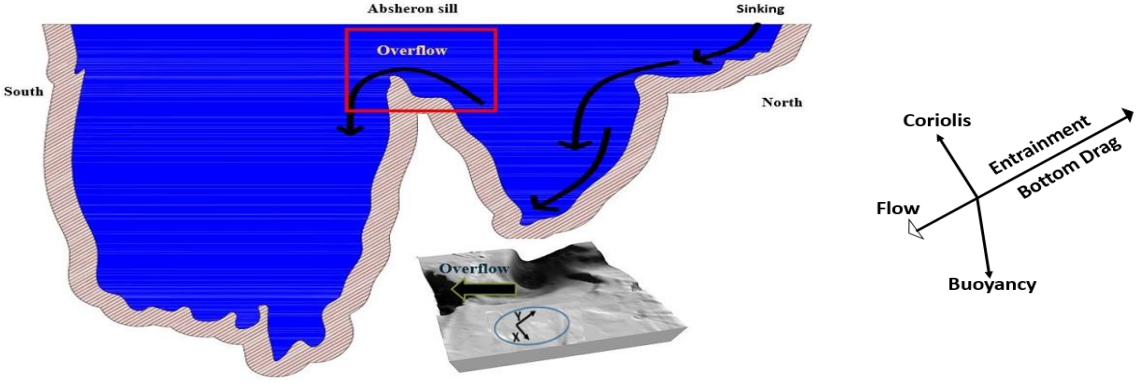

Figure 10: A schematic diagram of the sinking flow in the middle basin and the overflow current over Absheron sill (top), and topography around the sill in the middle of the Caspian Sea with the chosen coordinates (bottom).

Ocean Sci. Discuss., https://doi.org/10.5194/os-2018-13
Manuscript under review for journal Ocean Sci.
Discussion started: 16 February 2018

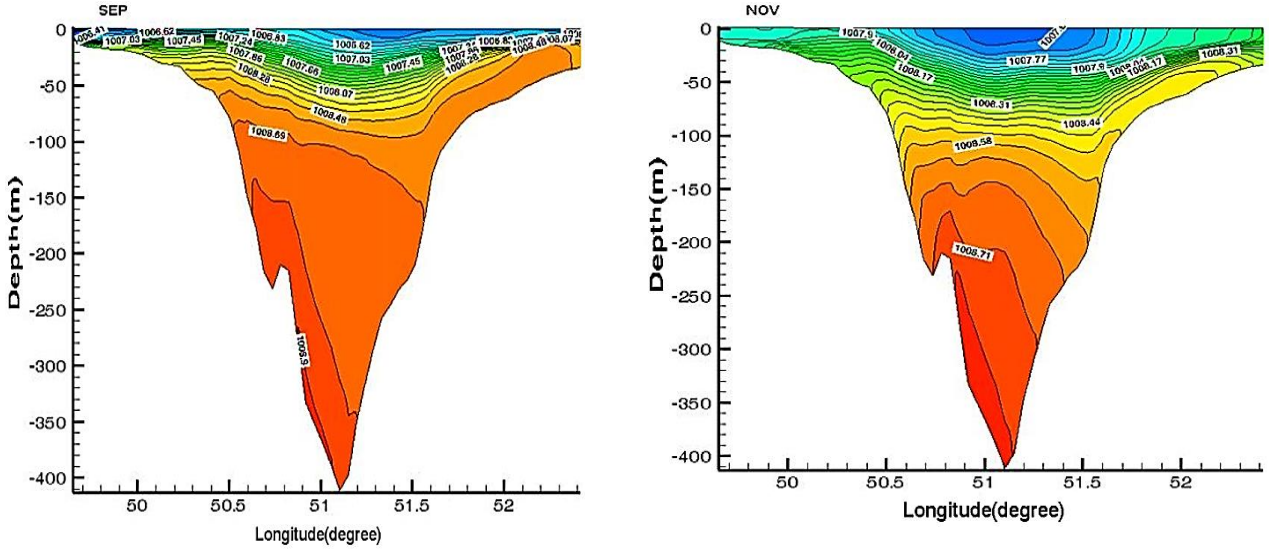

Figure 11: Simulated density fields along transect C in Sept. and Nov. 2004.

3.1.1 Estimation of drag coefficient and entrainment parameter

Johnson and Sanford (1992) estimated C_d=3×10^{-3} from the analysis of data from the Mediterranean outflow. Girton and Sanford (2003) used C_d=3×10^{-3} for Denmark Strait and Cheng et al (1999) studied the bottom roughness length and bottom shear stress in South San Francisco Bay and calculated C_d from 2×10^{-3} to 6×10^{-3}.In this study we have conducted the analysis using C_d=3×10^{-3}.

E is an entrainment speed and define as $E=E^*U$ where E^* is entrainment parameter that depends on a function of the layer Richardson number (Price and Bringer, 1994). Ri is the bulk Richardson number defined as $Ri = \frac{g'H}{U^2} cos\theta$, with U being the amplitude of layer velocity, θ is bottom slope. There are many methods to calculate E^* of which some are presented in table 1. Based on Ri for the outflow and due to the fact that Ri varies at different locations, we use two values for r_e. Based on table 1 and Ri >0.08, we used mean E^* based on formulas 2, 3, 4 and 5. In section 3.2 it will be discussed with more details.

Ocean Sci. Discuss., https://doi.org/10.5194/os-2018-13
Manuscript under review for journal Ocean Sci.
Discussion started: 16 February 2018

Table 1: Some of the published E^* equations based on Ri (Kashefipour et al, 2010)

Equation number	Researcher	Year	Equation
1	Ellison and Turner	1959	$E^*=\frac{0.08-0.1Ri}{1+5Ri}$
2	Ashida and Egashira	1977	$E^*=0.0015Ri^{-1}$
3	Garcia	1985	$E^*=\frac{0.075}{(1+718Ri^{2.4})^{0.5}}$
4	Kessel and Krancnburg	1996	$E^*=\frac{5.5\times10^{-3}}{3.6Ri-1+\sqrt{(3.6Ri-1)^2+0.15}}$
5	Karamzade	2004	$E^*=0.0021\ Ri^{-1.1238}$

3. 1. 2 *The result of the analytical model*

Figures 12 and 13 show that as the flow passes through the Strait, due to the Coriolis force it is deflected to the right. If initial velocity is greater, it moves farther along the meridian. The results show that at later times (especially for larger r_b and r_e) the flow moves a shorter distance in longitude and the direction of flow loses its sinusoidal oscillations (Figure 12 and Table 2). According to Table 2, the angle between the velocity and eastward horizontal is increased when compared with the initial velocity. After an initial acceleration, the flow oscillates a few times before adjusting to a flow at a small angle to the isobaths, depending on the bottom friction coefficients and entrainment (Figures 12 and 13). The results are based on uniform sloped bottom in the southern basin and initially the flow moves over the ramp. However, due to the bottom topography in southern basin and the narrow Apsheron strait, it is estimated that the flow after about 10 km is trapped. Due to a bottom slope of θ=0.02, the flow sinks approximately 180-200 m in the southern basin, as the numerical model confirms (Figures 6 and 7). In its following path, the flow have a different dynamic, thus another analytic model to describe the flow is presented (section 3.2).

Ocean Sci. Discuss., https://doi.org/10.5194/os-2018-13
Manuscript under review for journal Ocean Sci.
Discussion started: 16 February 2018

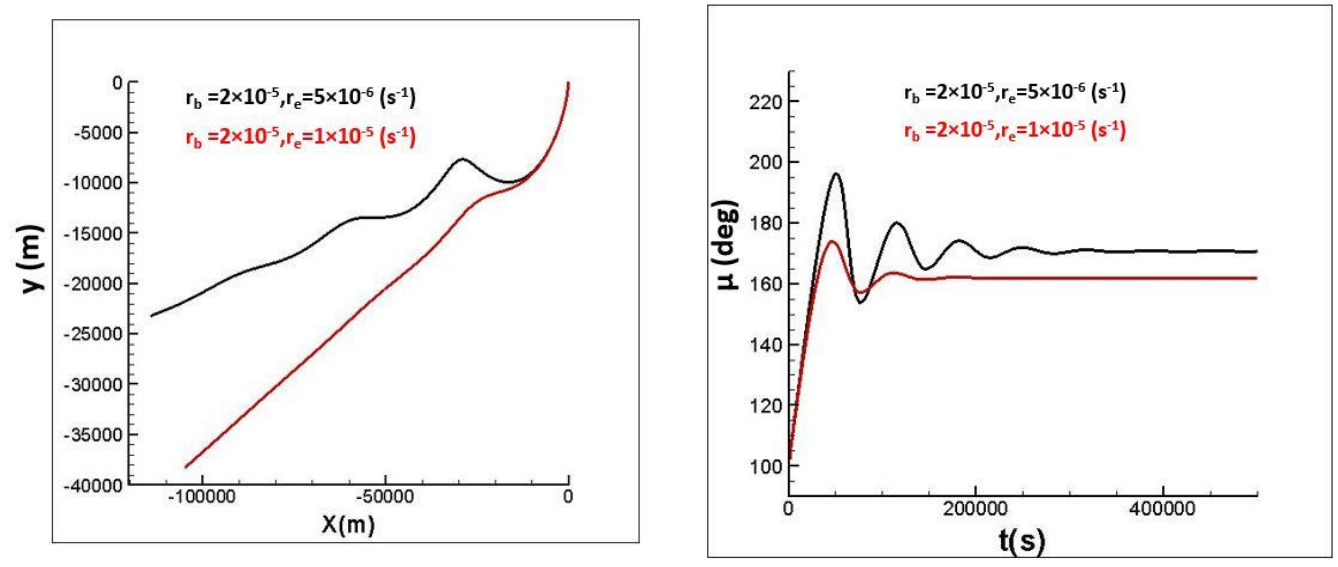

Figure 12: The flow paths (southwards, based on local coordinates used, see model descriptions above, t ~ 3 day) and its angle from eastward direction of the flow with different coefficients of entrainments.

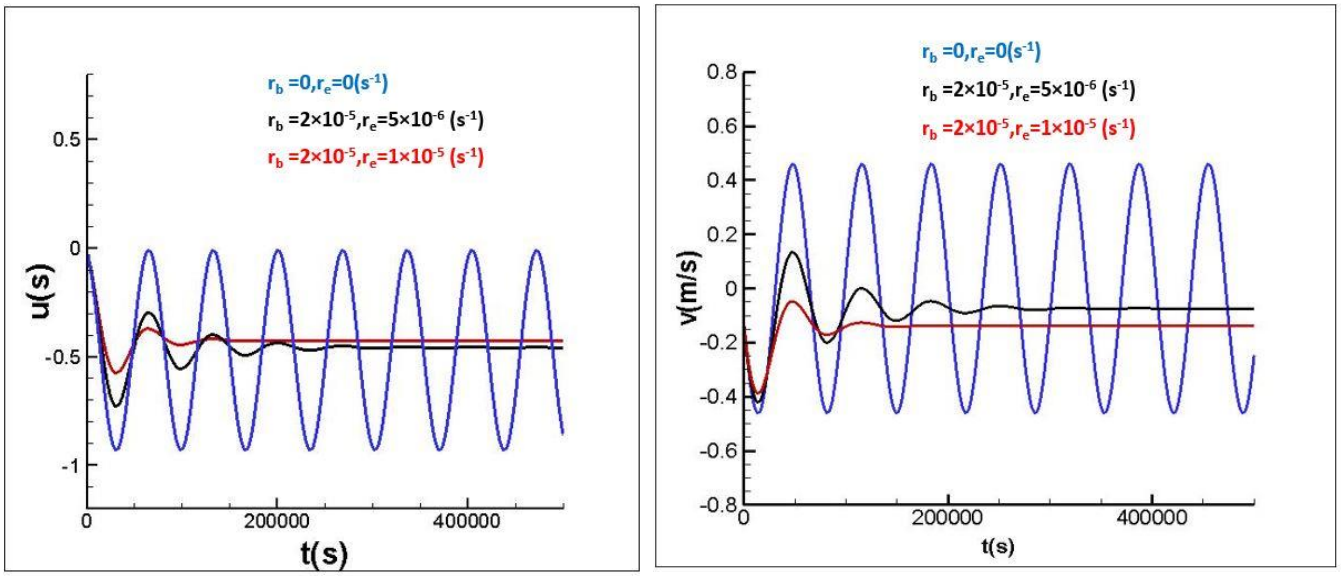

Figure 13: Comparison of the velocity components with different coefficients of entrainments.

Ocean Sci. Discuss., https://doi.org/10.5194/os-2018-13
Manuscript under review for journal Ocean Sci.
Discussion started: 16 February 2018

Table 2: Boundary current parameters and variables obtained from the numerical model (see text).

	g'(m/s^2)	v_p(m/s)	u_p (m/s)	$u_{t\to\infty}$ (m/s)	$v_{t\to\infty}$(m/s)	μ(deg)	λ (deg)
NOV	0.00222	-0.12	-0.044	-0.12	-0.119	160	107
JAN	0.00239	-0.133	-0.047	-0.13	-0.13	160	109.60
MAY	0.00251	-0.147	-0.031	-0.135	-0.135	160	101.91
SEP	0.00241	-0.19	-0.078	-0.132	-0.13	160	112.32

3. 2 Vorticity and potential vorticity (PV) over the sill

Here we consider the structure of fluid flowing on the sill in terms of its vorticity and PV. Falcini and Salusti (2015) presented an analytic model for the Sicily channel: vorticity and PV equations based on the stream-tube model (Smith, 1975; Killworth, 1977). To deal with this, they used (ξ, ψ) coordinate system, a modified form of that used by Astraldi et al. (2001). In this frame, ξ is the along-flow coordinate and ψ is the cross-flow coordinate (see Figure 1 in Smith, 1975). In this method, friction and mixing effects are considered for estimation of potential vorticity whereas other models assume a zero-PV flow (Whitehead et al., 1974). They presented two formulas to calculate vorticity and potential vorticity (5and 6). Formulas are based on a homogeneous bottom water vein (over bars indicate cross sectional averages).

$$\frac{\bar{\zeta}}{f}=\frac{\bar{u}_0}{\bar{u}}e^{-\int_0^{\xi}\frac{r}{\bar{u}}dx}\left(\frac{\bar{\zeta}_0}{f}+\frac{1}{\bar{u}_0}\int_0^{\xi}e^{\int_0^{x}\frac{r}{\bar{u}}dx'}\left[\frac{\bar{u}}{\bar{h}}\frac{\partial\bar{h}}{dx}-\frac{E}{\bar{h}}\right]dx\right) \qquad \textbf{(5)}$$

$$\Pi=e^{-\int_0^{\xi}\frac{\Gamma}{\bar{u}}dx}\left[\Pi_0-\int_0^{\xi}e^{\int_0^{x}\frac{\Gamma}{\bar{u}}dx'}\frac{r\zeta}{h\bar{u}}dx\right] \qquad \textbf{(6)}$$

Where $\Gamma=\frac{E}{h}$.

Here ζ and Π are respectively the mean relative vorticity and potential vorticity, h is the layer thickness and $\partial h/\partial x$ is slopes of the isopycnals, ζ_0 and $\overline{u_0}$ are receptively initial vorticity and velocity. To be applicable, some terms in Eq. 5 are considered cross sectional averages. Three terms are significant in vorticity: a stretching term, the entrainment effect, and friction. In 5 and 6, some symbols has been changed based on the present work. To estimate all parameters in these formulas, we use 5 transects from strait (I) to the southern area (V) (figure 16).Typically, for November in transect III Δh =180 m, Δx=38 km, $\bar{u}$=0.11 m/s, $\bar{h}$=180 m, are estimated. In the calculation of r_b, based on *Ri* number similar to that in section 3.1, $r_b=2\times10^{-5}$ (1/s) and $r_e=4\times10^{-6}$(for transect II), 8×10^{-7}(for transect III) are calculated based on formulas in table 1(figure 14). In transect IV and

Ocean Sci. Discuss., https://doi.org/10.5194/os-2018-13
Manuscript under review for journal Ocean Sci.
Discussion started: 16 February 2018

V, r_e~0 because of large *Ri*~ 40 to 50. Using Eqs. 5 and 6, profiles ζ and Π are plotted in figures 15 as functions of ξ along the steam tube.

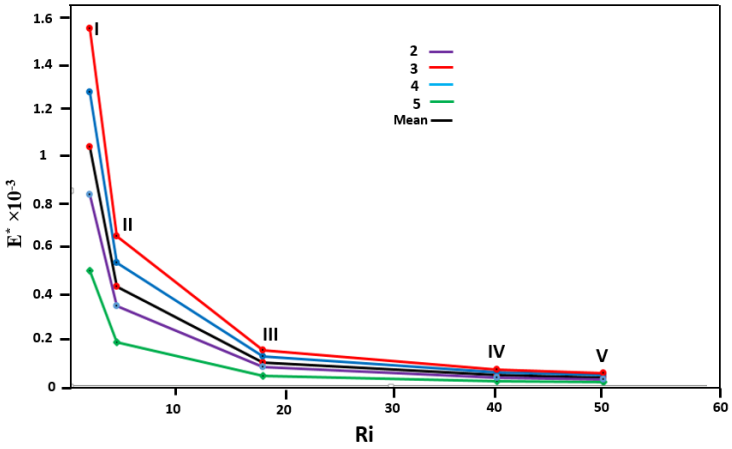

Figure 14: changes of entrainment coefficients based on different Richardson numbers for May in transects shown in figure 16. The formulas in table 1 are used to estimate E^* (the numbers refer to the equation numbers in table 1). To use E^* in Eq. 5and 6, mean values for E^* is also estimated (black).

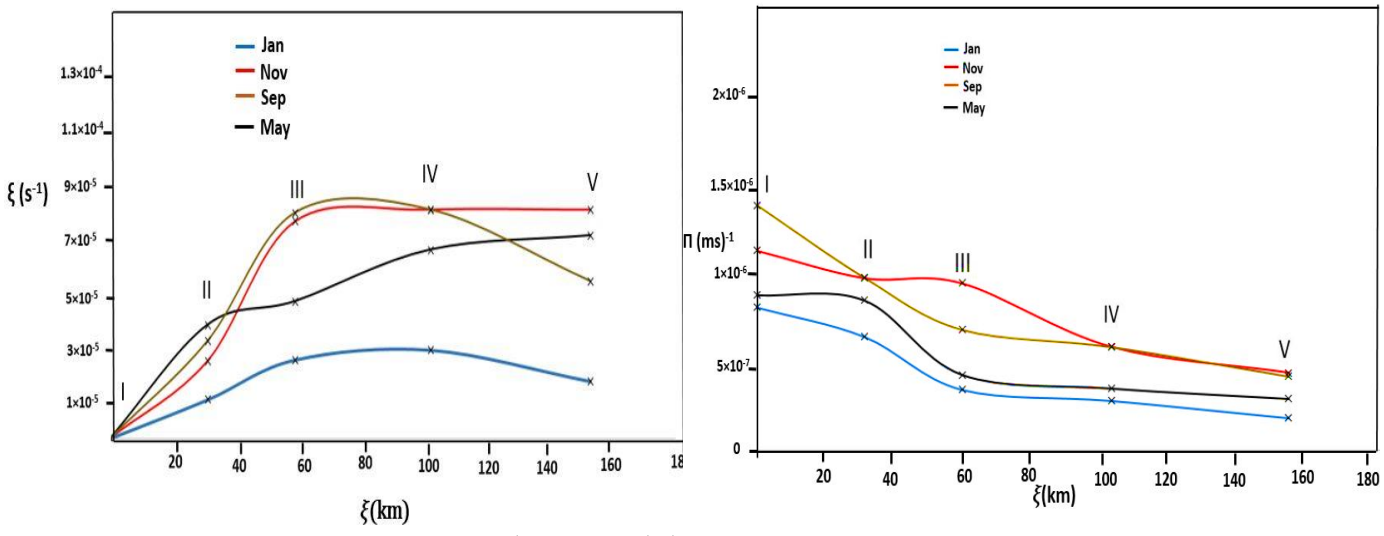

Figure 15: Changes in ζ (s^{-1}) and Π ($m^{-1}s^{-1}$) along the flow based on Eqs. 5 and 6.

Figure 15 illustrates that ζ values increase from I to V, because of stretching term in Eq. 5, although Sep and Jan values have different behaviour in transect IV to V. However after the transect III, the changes are not considerable, because the depth does not vary significantly (stretching term) and entrainment have been ignored as *Ri* is large after this transect. The month of November has the maximum value of vorticity of about 8.5×10^{-5} (1/s) in transect V, although the Jan. value has minimum vorticity among other months and also the changes are very little after transect III. When it comes to Π, the graph has a

Ocean Sci. Discuss., https://doi.org/10.5194/os-2018-13
Manuscript under review for journal Ocean Sci.
Discussion started: 16 February 2018

deceasing trend from I to IV, but after IV the Π values are almost constant. For example, the changes of Π over sill are about 7×10^{-7} ($m^{-1}s^{-1}$) and 4×10^{-7}($m^{-1}s^{-1}$) for Sep. and Jan. respectively, due to bottom friction and entrainment.

3.2.1 A model for the trapped flow

As the flow enters the southern Caspian Sea basin, it adjusts into an internal Quasi-geostrophic flow, because of topography in the southern Caspian basin (see Figure 16). When moving along the topography of the sea sloping sea bed, the governing equations of steady flow and similar assumptions as for the analytical model above, (see section 3.1) are as follows:

$$fv = g'\frac{\partial h}{\partial x} - r_b u$$
$$-fu = g'\frac{\partial h}{\partial y} - r_b v \qquad \textbf{(7)}$$

No mixing could exist due to flow entrainments near its boundaries due to Ri~50(E=0, or r_e=0). Where now u and v are respectively the eastward and northward velocity components (see Figure 16), g' is the reduced gravity, r_b is the friction coefficient (considered 0.00002 s^{-1}), and $\partial h/\partial x$, $\partial h/\partial y$ are slopes of the isopycnals of the overflow, related to the pressure gradient. From equation (7) it follows, assuming $\partial h/\partial y << \partial h/\partial x$:

$$\zeta = \frac{g'}{f + \frac{r_b^{\,2}}{f}}\frac{\partial^2 h}{\partial x^2} \qquad \textbf{(8)}$$

Potential vorticity is defined as:

$$\Pi = \frac{\zeta + f}{h} \qquad \textbf{(9)}$$

After substituting Eq. (8) in Eq. (9), an equation for h is obtained.

$$\frac{\partial^2 h}{\partial x^2} = \beta^2 h - \gamma$$

Where:

$$\beta^2 = \left(\frac{f + \frac{r^2}{f}}{g'}\right)\Pi$$

Ocean Sci. Discuss., https://doi.org/10.5194/os-2018-13
Manuscript under review for journal Ocean Sci.
Discussion started: 16 February 2018

$$\gamma = \left(\frac{f + \frac{r^2}{f}}{g'}\right) f$$

To estimate Π in transect D, we assume that $\Pi_V \sim \Pi_D$ because after the sill the flow depth is not changing and entrainment effect is almost zero. On the other hand, the bottom friction is important, however due to the short distance between D and V (figures 16 and 2), we use this assumption and overlook this effect. V is the downstream of the sill and D is the location at which the current is trapped by the topography.

The solution of *h* equation is as follows which is also shown in Figure 16:

$$h = c_1 e^{\beta x} + c_2 e^{-\beta x} + \frac{\gamma}{\beta^2} \qquad \textbf{(10)}$$

Where c_1 and c_2 are constants determined by the conditions that at the near-shore boundary ($x=0$) the flow vanishes, therefore *x* derivative of *h* near the shore is negligible. (See Figure 16, and Figure 17 which was used to derive values for these conditions); using these boundary conditions gives:

$$c_1 = c_2 = c$$

Hence, according to the equation, at $x=0$, $h_1 = 2c + \frac{\gamma}{\beta^2}$ and at $x=R$, $h_R = c\,(e^{\beta R} + e^{-\beta R}) + \frac{\gamma}{\beta^2}$ then:

$$R = \frac{1}{\beta} \cosh^{-1}\left(\frac{h_R - \frac{\gamma}{\beta^2}}{h_1 - \frac{\gamma}{\beta^2}}\right) \qquad \textbf{(11)}$$

Using equation 11 and also the result of the graph (figure17), the Rossby deformation radius are then calculated (Table 3).

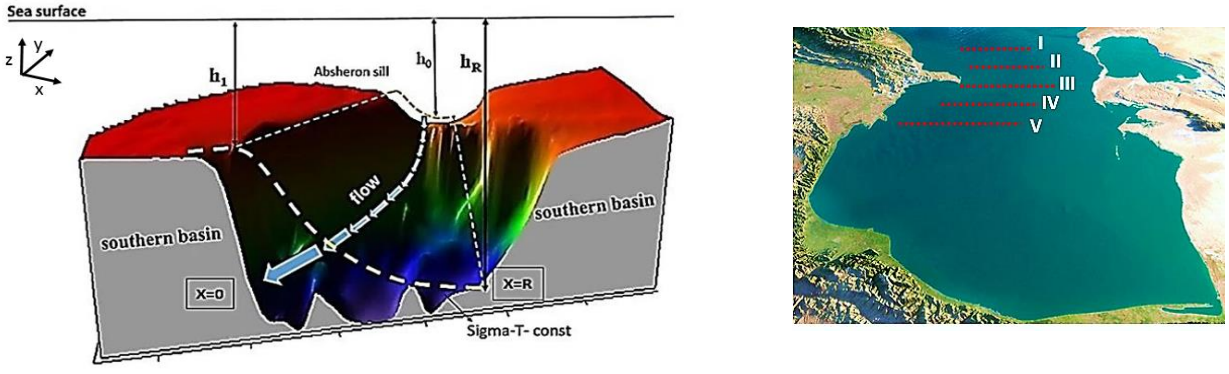

Figure 16: The parameters of the outflow model, a typical isopycnal surface is shown after the sill with corresponding *h* values found from the density fields such as shown in Figure 17(left) (Axes are in right-hand coordinates) and the locations of transects to estimate the changes of vorticity and PV (right).

Ocean Sci. Discuss., https://doi.org/10.5194/os-2018-13
Manuscript under review for journal Ocean Sci.
Discussion started: 16 February 2018

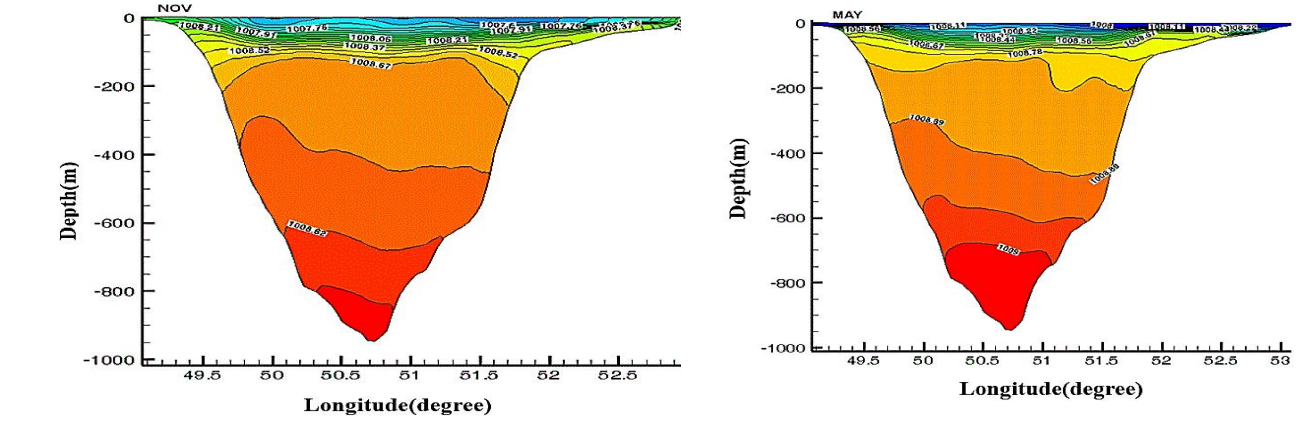

Figure 17: Density fields along transect D in May (right) and Nov. (left).

3. 2. 1.1 *The result of the analytical model*

This model is presented for the trapped flow after Absheron sill due to Coriolis effect. In this present work, due to the fact that we consider the friction and entrainment, the potential vorticity is not conserved, in contrast with the analysis of Bidokhti and Ezam (2009) for the Persian Gulf outflow. To calculate the changes in potential vorticity, we use the method of Falcini and Salusti used in Sicily Channel. Results show that the Rossby deformation radius (length, $\sim\beta^{-1}$) or the effective width of the flow directly depends on the drag coefficients and reduced gravity which varies for different seasons (based on Eq.11). The smallest and largest widths (Rossby lengths) of the flow are for January and May respectively (table 3). According to the results, Rossby deformation radius varies from 17 to 30 km in different seasons. The results illustrate that the decrease in potential vorticity increases the flow Rossby deformation radius, which means that when we use initial vorticity on strait ($\Pi_I \sim \Pi_D$) the radius will decrease. For instance, in September we assume that the $\Pi_I \sim \Pi_D$ similar to previous work Bidokhti and Ezam (2009); the radius is calculated about 12 km. Due to the results, we can predict that Rossby deformation radius will increase in another location of the southern Caspian sea (near the Iranian coast), transect E in figure 2 because the bottom friction decrease Π_E rather than Π_D. The numerical model (figure 9) confirms this prediction. As a result, Eq.7 and 8 can predict the changes of vorticity correctly over and after the Absheron sill.

Ocean Sci. Discuss., https://doi.org/10.5194/os-2018-13
Manuscript under review for journal Ocean Sci.
Discussion started: 16 February 2018

Table 3: Boundary trapped current model parameters (see Figure 16 and transect D in figure 17) and values of *R*.

	h_0(m)	h_1(m)	h_R (m)	R (km)
NOV	120	270	400	17
JAN	150	440	485	15
MAY	110	300	400	30
SEP	140	430	570	25

3. 3 Flushing times and the volumes of dense water calculations

In this section, as we derive the parameters of the overflow, a relation is presented for the calculation of the abyssal volume flow rate between the two basins of the Caspian Sea via the Absheron Strait. This is given by (12) in which *v* is the mean magnitude of geostrophic velocity of the overflow and *ds* is an element of its cross section area.

$$Q_V = \int v\,ds \qquad \textbf{(12)}$$

Due to the parabolic form of the bottom topography of Absheron Strait, its geometry of the dense overflow in this valley like shape (Figure 18) can be given by:

$$\begin{aligned} Z &= ax^2 + bx + c \\ h &= Ae^{-\alpha x} \end{aligned} \qquad \textbf{(13)}$$

Where *a*, *b*, *c*, *A*, and α are assumed to be constant. Due to the fact that *Z* and *h* (isopycnal line) in graph (Figure 18) are from L_1 to L_2 we can calculate *h* and *Z* values at (x=L_1) and (x=L_2), Substituting Eq. (13) in Eq. (12) and using these assumptions and that *v*, the geostrophic flow speed, is given by the slope of *h* in *x* direction, we have:

$$Q_V = \frac{g'}{f}\frac{H_1 - H_2}{L_2 + L_1}\left[\left(-\frac{A}{\alpha}(e^{-\alpha L_2} - e^{\alpha L_1})\right) - \frac{a}{3}(L_2^3 + L_1^3) - \frac{b}{2}(L_2^2 - L_1^2)\right] \qquad \textbf{(14)}$$

Where:

$$a = \frac{H_2 L_1 + H_1 L_2}{L_1(L_2^2 + L_1 L_2)}$$

$$b = \frac{H_2 L_1 + H_1 L_2}{L_2^2 + L_1 L_2} - \frac{H_1}{L_1}$$

If we assume that $L = \frac{|L_1| + |L_2|}{2}$, we have

Ocean Sci. Discuss., https://doi.org/10.5194/os-2018-13
Manuscript under review for journal Ocean Sci.
Discussion started: 16 February 2018

$$Q_V = \frac{g'}{f}\frac{H_1 - H_2}{L_2 - L_1}\left[\frac{2A}{\alpha}\sinh(\alpha L) - \frac{2}{3}aL^3\right] \qquad \textbf{(15)}$$

Where:

$$a = \frac{H_2 + H_1}{2L^2}$$

$$b = \frac{H_2 - H_1}{2L}$$

$$A = \frac{H_1}{e^{\alpha L}}$$

$$\alpha = -\frac{1}{2L} Ln \frac{H_2}{H_1}$$

Although the minimum of Z is not exactly at x=0, it does not create large errors. To show this reality, the Q_V is calculated separately with Eq. 14 and 15. The results show that the error is about 2-5 percent rather than using any assumptions (Eq.14). To calculate the mean monthly volume flow rate of the deep current that enters the southern basin of the Caspian Sea, we assume that its density is greater than 1008.78 kg/m^3, the average density (for different seasons) of the flow upper boundary (e.g. Figure 19) and use equation (17) and figure 19 for this purpose.

For the times that the middle and southern basins are filled, first the volumes of middle (V_M), and southern (V_S) basins (see Figure 18) below three levels (z= 0, z= -100, and z= -150 m, the approximate depth of the Absheron sill that is more appropriate only for southern basin) are calculated, then if we assume the same annual mean value Q_V for both basins, these filling times are estimated. The results of these calculations and comparisons between them in different seasons are given in Tables 4 and 5. The results show that the maximum and minimum flow rates of abyssal water that enter the Southern Caspian Sea are in May and November respectively.

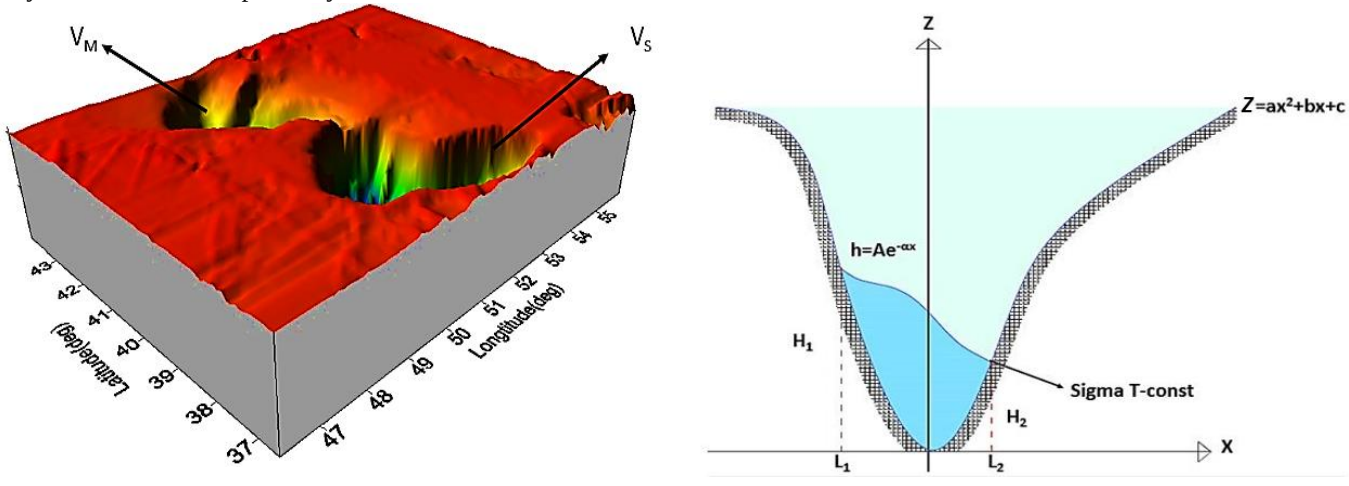

Figure 18: The modelling bathymetry used and the scheme of the topography with a typical isopycnal and model parameters.

Ocean Sci. Discuss., https://doi.org/10.5194/os-2018-13
Manuscript under review for journal Ocean Sci.
Discussion started: 16 February 2018

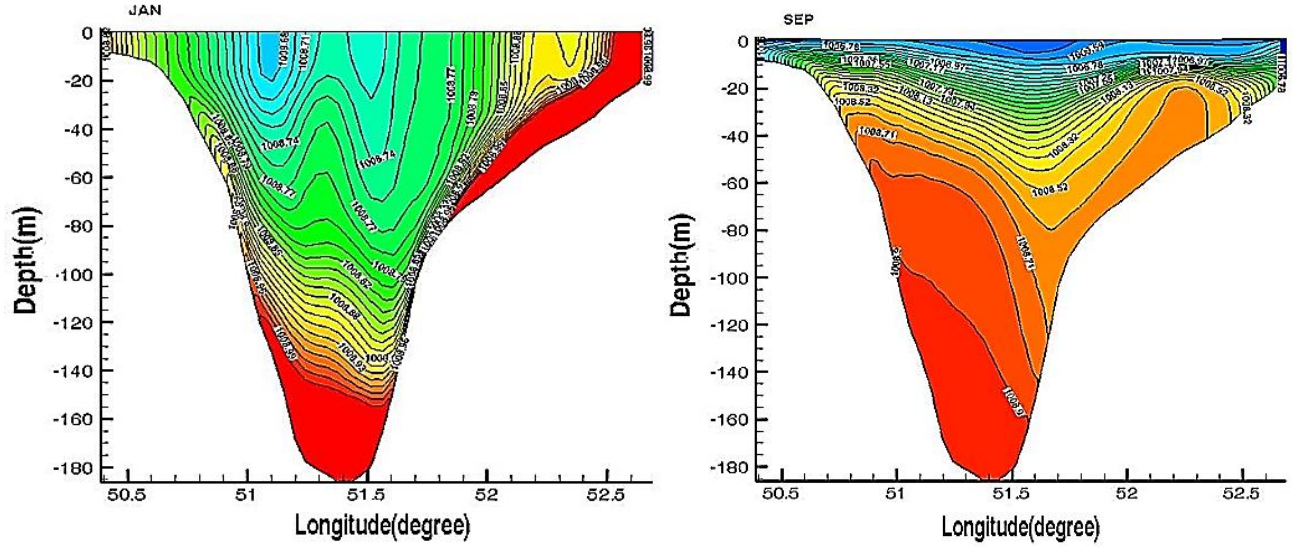

Figure 19: Typical density fields along transect A for Jan. (left) and Sept. (right) from which we calculate the flow rates.

Table 4: The model boundary current parameters (1 *Sv*=10^6 m^3/s) for different months.

	H_1 (m)	H_2 (m)	$2L$ (m)	Q_V (Sv)
NOV	55	10	19000	0.016
JAN	145	85	32000	0.115
MAY	145	55	34000	0.146
SEP	135	45	27500	0.116

Table 5: Flushing times of the middle (T_M) and the southern (T_S) basins (using an annual average volume flow rate, Q_V) below three levels.

Level	V_M ($m^3\times10^{13}$)	V_S ($m^3\times10^{13}$)	T_M (year)	T_S (year)
***z*=0 (sea surface)**	2.55	5.12	8.35	16.77
***z*=-100**	1.09	4.13	3.57	13.5
***z*=-150**	0.36	3.62	1.17	11.85

4. Conclusions

The results of observations and numerical simulations showed that there is an abyssal flow from the middle to the southern basins of the Caspian Sea. The density difference between the deeper water of the middle basin and that of southern basin leads to an overflow gravity current over the Absheron sill. This difference is mainly due to the temperature difference between deeper parts of these two basins, as a result of cold water initially sinking in the northern part of this Sea, at about 48 degrees

latitude, that fills first the middle basin and then overflows towards the southern basin. In the autumn and winter, surface water cools, its density is increased and then sinks to the deep part of the middle basin, as the deep convection process in high latitude oceans. Winter storms and cold wind provide the cooling of this rather high-latitude shallow water in the northern basin.

Analytical models for the gravity driven flow over the sloped bed of the Absheron sill and that of subsequent trapped flow, were used to estimate typical mass transport and flushing times of the deep water basins of this Sea. The model for the gravity driven flow over a sloped bed has inertial, Coriolis and frictional forces included. In its initial stage the flow has some oscillations of inertial type with typical local inertial period at this latitude. After this varying behaviour, the flow adjusts itself moving south as a gravity driven topographically trapped current, spiralling into deeper parts due to bottom friction and entrainment. It always tends to move toward the western shores of this Sea, mainly due to the Coriolis force that shifts it to the right. Such flow is important in the abyssal circulation and ventilation of the deep southern basin of the Caspian Sea. The model for the determining Rossby length of the flow showed that it varies for different seasons. For vorticity and potential vorticity of the flow, the formulas which are presented by Falcini and Salusti (2015) are used to estimate the changes of relative vorticity and potential vorticity over Absheron sill, that are used in the analytical trapped current.

Results also showed that nearly 3.05×10^{12} m^3 of water per year by this abyssal flow can enter the Southern basin giving a typical flushing time of about 15 to 20 years which are of the same order as those estimated by Peeters et al. (2000), as the southern Caspian basin ecosystem is strongly dependent on this flow.

The northern and middle Caspian Sea basins have become important areas for oil and gas explorations (especially the Absheron shallow Strait area) and marine transport nowadays. Since the Caspian Sea is an enclosed sea, the adverse effects of such activities may particularly affect the deep part of these Caspian Sea basins. For this reason, it is recommended that more detailed observational data are collected in the deep parts of the southern and middle basins of the Caspian Sea, by joint projects with neighbouring countries. More extensive and high resolution observational data and numerical simulations are required to find more details of the outflow structure over and around the Absheron sill (Strait) and the deeper parts of this Sea basins.

References

Arakawa, A. & Suarez, M. J. (1983). Vertical differencing of the primitive equations in sigma coordinates. *Monthly Weather Review, 111*(1), 34-45.

Astraldi, M., Gasparini, G. P., Gervasio, L. & Salusti, E. (2001). Dense water dynamics along the Strait of Sicily (Mediterranean Sea). Journal of Physical Oceanography, 31(12), 3457-3475.

Ashida, K. & Egashira, S. (1975, May). Basic study on turbidity currents. In Proceedings of the Japan Society of Civil Engineers (Vol. 1975, No. 237, pp. 37-50). Japan Society of Civil Engineers.

Aubrey, D.G., Glushko, T.A. & Ivanov, V.A. (1994). North Caspian Basin: Environmental status and oil and gas operational issues, *Report for Mobil-oil, 650 pages.*

Aubrey, D.G. (1994). Conservation of biological diversity of the Caspian Sea and its coastal zone. A proposal the Global Environment Facility, *Report to GEF, 250 pages.*

Baringer, M. O. N. & Price, J. F. (1997). Mixing and spreading of the Mediterranean outflow. *Journal of Physical Oceanography*, *27*(8), 1654-1677.

Bidokhti, A. A. & Ezam, M. (2009). The structure of the Persian Gulf outflow subjected to density variations. *Ocean Science*, *5*(1), 1-12.

Bondarenko, A. L. (1993). Currents of the Caspian Sea and Formation of Salinity of the Waters of the North Part of the Caspian Sea [in Russian], *122 pp., Nauka, Moscow, Russia.*

Britter, R. E. & Linden, P. F. (1980). The motion of the front of a gravity current travelling down an incline. *Journal of Fluid Mechanics*, *99*(3), 531-543.

Cheng, R. T., Ling, C. H., Gartner, J. W. & Wang, P. F. (1999). Estimates of bottom roughness length and bottom shear stress in South San Francisco Bay, California. *Journal of Geophysical Research: Oceans*, *104*(C4), 7715-7728.

Dickson, R. R., Gmitrowicz, E. M. & Watson, A. J. (1990). Deep-water renewal in the northern North Atlantic. *Nature*, *344*(6269), 848-850.

Ellison, T. H. & Turner, J. S. (1959). Turbulent entrainment in stratified flows. *Journal of Fluid Mechanics*, *6*(3), 423-448.

Falcini, F. & Salusti, E. (2015). Friction and mixing effects on potential vorticity for bottom current crossing a marine strait: an application to the Sicily Channel (central Mediterranean Sea). Ocean Science, 11(3), 391-403.

Fogelqvist, E., Blindheim, J., Tanhua, T., Østerhus, S., Buch, E. & Rey, F. (2003). Greenland–Scotland overflow studied by hydro-chemical multivariate analysis. *Deep Sea Research Part I: Oceanographic Research Papers*, *50*(1), 73-102.

García, M. H. (1993). Hydraulic jumps in sediment-driven bottom currents. Journal of Hydraulic Engineering, 119(10), 1094-1117.

Ghaffari, P. & Chegini, V. (2010). Acoustic Doppler Current Profiler observations in the southern Caspian Sea: shelf currents and flow field off Feridoonkenar Bay, Iran. *Ocean Science*, *6*(3), 737.

Ghaffari, P., Isachsen, P. E. & LaCasce, J. H. (2013). Topographic effects on current variability in the Caspian Sea. *Journal of Geophysical Research: Oceans*, *118*(12), 7107-7116.

Girton, J. B. & Sanford, T. B. (2003). Descent and modification of the overflow plume in the Denmark Strait. *Journal of Physical Oceanography*, *33*(7), 1351-1364.

Griffiths, R. W. (1986). Gravity currents in rotating systems. *Annual Review of Fluid Mechanics*, *18*(1), 59-89.

Gunduz, M. & Özsoy, E. (2014). Modelling seasonal circulation and thermohaline structure of the Caspian Sea. *Ocean Science*, *10*(3), 459-471.

Ibrayev, R. A., Özsoy, E., Schrum, C. & Sur, H. I. (2010). Seasonal variability of the Caspian Sea three-dimensional circulation, sea level and air-sea interaction. *Ocean Science*, *6*(1).

Ismailova, B. B. (2004). Geoinformation modeling of wind-induced surges on the northern–eastern Caspian Sea. *Mathematics and Computers in Simulation*, *67*(4), 371-377.

Johnson, G.C. and Sanford, T.B. (1992). Bottom and interfaeial stresses on the Mediterranean outflow. Tenth Symposium on Turbulence and Diffusion. Portland, Oregon. *American MeteorologicalSociety, 105-106.*

Kara, A. B., Wallcraft, A. J., Metzger, E. J. & Gunduz, M. (2010). Impacts of freshwater on the seasonal variations of surface salinity and circulation in the Caspian Sea. *Continental Shelf Research*, *30*(10), 1211-1225.

Karamzadeh, N. (2004). Experimental investigation of water entrainment into density current. M. Sc. Thesis, Shahid Chamran University, Ahvaz, Iran.

Kashefipour, S., Kooti, F. & Ghomeshi, M. (2010, June). Effect of reservoir bed slope and density current discharge on water entrainment. In Environmental Hydraulics, Two Volume Set: Proceedings of the 6th International Symposium on Enviornmental Hydraulics, Athens, Greece, 23-25 June 2010 (p. 195). CRC Press.

Kessel, T. V. & Kranenburg, C. (1996). Gravity current of fluid mud on sloping bed. Journal of Hydraulic Engineering, 122(12), 710-717.

Killworth, P. D. (1977). Mixing of the Weddell Sea continental slope. Deep Sea Research, 24(5), 427-448.

Luyten, P. J., Jones, J. E., Proctor, R., Tabor, A., Tett, P. & Wild-Allen, K. (1999). COHERENS- A coupled hydrodynamical-ecological model for regional and shelf seas: user documentation, MUMM Rep., *Management Unit of the Mathematical Models of the North Sea.*

Mazaheri, S., Kamranzad, B. & Hajivalie, F. (2013). Modification of 32 years ECMWF wind field using QuikSCAT data for wave hindcasting in Iranian Seas. *Journal of Coastal Research*, *65*(sp1), 344-349.

Peeters, F., Kipfer, R., Achermann, D., Hofer, M., Aeschbach-Hertig, W., Beyerle, U. & Fröhlich, K. (2000). Analysis of deep-water exchange in the Caspian Sea based on environmental tracers. *Deep Sea Research Part I: Oceanographic Research Papers*, *47*(4), 621-654.

Price, J. F. & Baringer, M. O. N. (1994). Outflows and deep water production by marginal seas. *Progress in Oceanography*, *33*(3), 161-200.

Shiea, M., Chegini, V. & Bidokhti, A. A. (2016). Impact of wind and thermal forcing on the seasonal variation of three-dimensional circulation in the Caspian Sea, IJMS, Vol. 45 (05), 671-686.

Smith, P. C. (1975, December). A streamtube model for bottom boundary currents in the ocean. In *Deep Sea Research and Oceanographic Abstracts* (Vol. 22, No. 12, pp. 853-873), Elsevier.

Terziev, F. S., Kosarev, A. & Kerimov, A.A. (1992). The Seas of the USSR. Hydrometeorology and Hydrochemistry of the Seas, vol. VI, the Caspian Sea, Issue 1: Hydro meteorological Conditions, Gidrometeoizdat, St. Petersburg, Russia.

Whitehead, J. A., Leetmaa, A. & Knox, R. A. (1974). Rotating hydraulics of strait and sill flows. *Geophysical and Astrophysical Fluid Dynamics*, *6*(2), 101-125.